Chapter 2

SUPERCONTINUUM AND HIGH-ORDER HARMONICS

"Extreme" Coherent Sources for Atomic Spectroscopy and Attophysics

Marco Bellini*
Istituto Nazionale di Ottica Applicata (*INOA*)
Largo Fermi 6, 50125 Florence, Italy
bellini@inoa.it

Abstract Simple experiments, set up to investigate how the coherence properties of short and intense laser pulses are transferred to radiation generated in extremely nonlinear interactions with matter, have given access to a wealth of new information and have allowed unexpected advances in several different fields. Here, we review some of these experiments and discuss their implications for the development of new methods in ultra-high spectral and temporal resolution studies of matter.

Keywords: Ultrashort laser pulses, nonlinear optics, high-order harmonic generation, extreme ultraviolet, supercontinuum generation, frequency comb, attosecond pulses.

1. INTRODUCTION

Ultrashort laser pulses are an invaluable tool to study ultrafast atomic and molecular events on a femtosecond timescale. The advent of mode-locking techniques has allowed the generation of pulses whose duration comprises just a few oscillations of the optical field, while the development of chirped-pulse-amplification methods has opened the way to ultra-intense laser pulses, which are capable of driving extremely nonlinear phenomena in matter. As a matter of fact, the latest major developments in the field of laser physics are a direct

*Also at European Laboratory for Nonlinear Spectroscopy (LENS) and Istituto Nazionale per la Fisica della Materia (INFM), Florence, Italy.

outcome of the parallel evolution of both techniques, and have recently led to the generation of intense few-cycle pulses and to the first glimpses on a new scientific era – attophysics.

These latest achievements, however, wouldn not have been possible without a number of important new discoveries, which have helped to clarify the scientific background and have provided new essential tools for the development of the final techniques. The generation of attosecond pulses, in particular, relies both on a complete understanding of well-developed methods for the production of high-order laser harmonics and on the availability of few-cycle intense laser pulses with an accurately controlled absolute phase.

In this chapter, I will focus on studies performed in our laboratory on the radiation produced in the extreme ultraviolet (XUV) by the process of high-order harmonic (HOH) generation and on the white-light supercontinuum (SC) obtained when intense laser pulses impinge on transparent materials. I will show that, using simple experimental ideas to investigate the coherence properties of these two different kinds of "extreme" light sources, we were able to obtain interesting and unexpected results in fields that could initially appear to be almost completely unrelated, like strong-field atomic physics and high-precision optical metrology. Finally, I will merge these two apparently distant subjects in order to give just a quick glimpse on how these experiments played a fundamental role in the race toward the breaking of the femtosecond barrier and the development of attophysics.

2. HIGH-RESOLUTION SPECTROSCOPY WITH ULTRASHORT PULSES

Exploiting the extremely high peak intensities characteristic of ultrashort laser pulses to excite multiphoton processes or to drive highly nonlinear phenomena (and generate new wavelengths, for example), while maintaining the high resolution characteristic of CW sources to investigate very narrow spectral structures of atoms or molecules, is one of the forbidden dreams of the laser experimentalist. Unfortunately, the two conditions of ultrashort pulse duration and high spectral resolution normally appear in striking contrast, since short pulses invariably correspond to broad spectral bandwidths that limit the frequency resolution to the inverse of the pulse duration (see Fig. 2.1 a). However, if pairs of time-delayed and phase-locked pulses (like those generated by splitting a single laser pulse by means of a Michelson interferometer) are used, a simple Fourier transformation shows that the corresponding spectrum maintains the broad bell-shaped envelope, but also acquires a sinusoidal modulation with a spectral period given by the inverse of the temporal separation τ between

the two pulses (see Fig. 2.1 b). In the ideal case, where the two time-delayed pulses with electric fields $E_1(t)$ and $E_2(t+\tau)$ are perfectly phase-locked, their combined spectrum is easily found to be

$$I_t(\omega,\tau) = I_1(\omega) + I_2(\omega) + 2\sqrt{I_1(\omega)I_2(\omega)}\cos(\omega\tau), \tag{2.1}$$

which reduces to

$$I_t(\omega,\tau) = 2I(\omega)(1+\cos(\omega\tau)) \tag{2.2}$$

in the case of equal pulse intensities $I(\omega) = I_1(\omega) = I_2(\omega)$.

It is this $1/\tau$ fringe period that now sets the instrumental resolution and allows one, in principle, to investigate very fine spectral features if a long time delay τ is available[1].

The idea of using a pair of phase-locked pulses in order to achieve better spectral resolution can also be extended by the use of longer sequences of equally time-delayed and phase-locked pulses. The spectrum that one obtains in this case still exhibits the broad bandwidth related to the short pulse duration, but is now modulated in a sharper and sharper fashion as longer pulse sequences are used (see Fig. 2.1 c). In the case of N equally spaced (by a delay τ) and phase-locked pulses, the textbook solution for the corresponding spectrum is given by the expression

$$I(\omega,\tau) = I_0(\omega)\left(\frac{\sin N\omega\tau/2}{\sin\omega\tau/2}\right)^2 \tag{2.3}$$

and the spectral interference pattern is the well-known array of intense and sharp interference maxima at $\omega_n = n\frac{2\pi}{\tau}$, with some small residual modulations in between. In the ideal limit of an infinite train of phase-locked and equally-spaced pulses ofduration τ_p, the resulting spectrum essentially consists of a "comb" of infinitely sharp lines, equally separated by a frequency spacing corresponding to the inverse of the inter-pulse period and extended over a frequency range inversely proportional to τ_p. The advantages of such a peculiar spectral distri-

[1]The first demonstration of high-resolution spectroscopy of multiphoton atomic transitions with ultrashort pulses dates back to 1996, when we showed that it was indeed possible to measure line splittings (the hyperfine separation of the $8S_{\frac{1}{2}}$ state in cesium in that case) in a two-photon transition with a spectral resolution much better than that given by the single-pulse spectral width [1]. This is the same principle of Fourier Transform Spectroscopy that normally uses broad-bandwidth CW sources to perform medium-to-high resolution studies in the medium- and far-infrared. One of the advantages of employing this technique with short pulses is that one can now use their high peak intensities to move to different spectral regions or to investigate new transitions involving two or more photons [2].

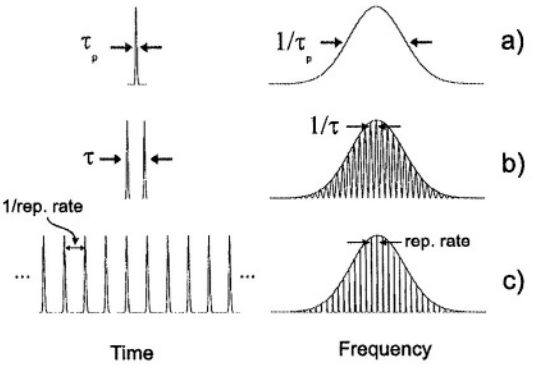

Figure 2.1. A single laser pulse has a frequency bandwidth which scales with the inverse of its duration τ_p (a). If one uses a pair of phase-locked pulses, delayed by a time τ, the resulting spectrum maintains the broad envelope of width $1/\tau_p$ but with a sinusoidal modulation of spectral period $1/\tau$ (b). This width sets the new instrumental resolution. If one uses an infinite sequence of pulses, locked in phase and equally delayed in time by the interval τ, the spectrum breaks up in a "comb" of very narrow lines (the "teeth") equally spaced by a frequency interval $1/\tau$ (c).

bution are evident: this spectral comb can be used as a precise ruler to measure unknown frequency intervals in a relatively simple way. By locking two laser lines to two different "teeth" of the comb, and by counting the integer number of interposed teeth, one can immediately obtain the unknown frequency gap, if the separation between the teeth is well known. A mode-locked laser is a natural way for generating such an ideally infinite sequence of time-delayed pulses with a well-defined phase relationship [3]. Its spectrum (given by the set of equally-spaced longitudinal modes of the cavity) is a broad comb of frequencies with a mode separation equal to the measurable and controllable pulse repetition rate (see Fig. 2.1 c). The largest frequency gap that can be bridged with such a comb is determined by the inverse of the pulse duration τ_p (if the pulse is Fourier transform-limited), but it can be widely extended if nonlinear interactions are used to broaden the spectrum.

In any case, one of the essential requirements for these novel spectroscopic techniques to work is that the phase coherence between the pulses in the sequence is accurately preserved. The experiments described below were mainly aimed to check this coherence preservation in the particular highly-nonlinear processes of HOH and SC generation, but their results went far beyond the initial scope. Besides demonstrating phase coherence in both cases and achieving high-resolution with a Ramsey-type XUV spectroscopy, we clarified the microscopic processes of high-order harmonic generation and established the

basis for the invention of the femtosecond frequency combs, the two essential ingredients for the generation of attosecond pulses.

3. HIGH-ORDER HARMONICS

3.1 Basic Principles

Pulses with frequencies which are odd-order harmonics of the fundamental laser frequency can be generated by the interaction of short and intense laser pulses with the atoms of a supersonic gas jet. The most impressive characteristic of HOH is the existence of a *plateau* in the emitted spectrum [4, 5]. At variance with the usual exponential decay of the conversion efficiency for increasing harmonic orders (as found with the perturbative treatment of nonlinearities in a medium), the HOH spectrum only presents such an exponential decay for the first few harmonics, being quickly replaced by a region of almost constant efficiency (the *plateau*), which may comprise many successive orders. Depending on the wavelength, duration and peak intensity of the pulses, and on the ionization potential of the atoms, very high orders can be efficiently generated at wavelengths down to the XUV or to the soft X-ray regions. The maximum extension of the *plateau* is defined by the so-called *cut-off* energy, which is normally found to follow a rather simple law:

$$E_{cut-off} \approx I_P + 3.2\,U_P, \tag{2.4}$$

where I_P is the ionization potential of the gas, and $U_P \propto I\lambda^2$ (with I and λ the peak intensity and wavelength of the driving laser, respectively) is the so-called ponderomotive energy (see Ref. [6] for a recent review).

3.2 Phase Coherence in Harmonic Generation

Although harmonic sources are extremely appealing due to the lack of other easily accessible alternatives in these spectral regions, the extremely broad bandwidth associated with their short pulse duration seems to prevent their use for spectroscopy. In fact, even if some low-to-medium-order harmonics can be generated with pump pulses in the nanosecond and picosecond range [7–9], allowing one to keep a good spectral resolution for selected applications, higher-order harmonics can only be created at intensities above 10^{13} W/cm^2 by ultrashort laser pulses. A 100 fs pulse is already characterized by a spectral width in the THz range.

A way to overcome this limit is with the application of the two-pulse technique, described above, to the harmonic radiation, by splitting and delaying the

XUV pulses by means of a Michelson interferometer before sending them to the samples under study. Unfortunately, the use of this technique with HOH pulses is far from straightforward, mainly because good interferometers cannot be built to work in the XUV due to the lack of suitable optics. One can think of solving this problem by moving the interferometer in the path of the laser beam, in order to create two phase-locked and time-delayed pump pulses that would then generate equally phase-related XUV pulses, but the question at this point concerns the preservation of the phase lock in the generated pulses: if the process of HOH generation were an incoherent one, no phase relationship could be preserved between the XUV pulses, and such a scheme for spectroscopy with harmonics would be useless.

A simple way to test the mutual phase coherence between the harmonic pulses produced by phase-locked pump pulses is to generate them in two separate spatial regions and look for interference fringes in the far field: the existence of a stable interference pattern would show that the two secondary sources have preserved a memory of the phases of their parent pulses[2]. A first experiment concerning HOH was carried out in Lund, where harmonics were generated by focusing 30 ps laser pulses into an argon gas jet [11]. After the focusing lens, the laser pulses were split and given a slight fixed displacement (both in space and time) thanks to the walk-off in a birefringent plate, and a common polarization component was selected before entering the interaction region. Harmonics were then generated in two different positions in the gas jet and we looked for interference fringes in the far field, after spectral dispersion produced by a grating. Nice, stable and highly-contrasted fringes were unexpectedly observed, indicating that the generation process was not as phase-destructive as initially thought, and demonstrating that harmonic generation could become a suitable source for XUV interferometry [12]and high-resolution two-pulse spectroscopy.

A second experiment was later performed at LENS using a Michelson interferometer to split and delay the laser pulses (only about 100 fs long, in this case) so that their temporal and spatial separation in the focus could be carefully adjusted and controlled [13]. Very clear interference fringes were again observed on the Micro-Channel-Plate detector placed beyond the exit slit of the vacuum monochromator, and the temporal coherence of the harmonics could be determined by observing the decay of the fringe visibility as a function of the

[2]A preliminary experiment with the third harmonic generated in air gave very interesting and encouraging indications [10], although it was not possible to directly extrapolate the results to higher orders and the general thought was that, in such a case, the generation process would have completely messed up the phases of the harmonic pulses, destroying any interference.

inter-pulse delay. Almost transform-limited XUV pulses with coherence times of the order of the expected duration of the harmonics themselves (about 40 fs) were generated, showing that not only was the phase not scrambled in the process, but also that a negligible frequency chirp was imparted to the secondary pulses.

While doing this, we also discovered some new and unexpected features: the presence of two clearly distinct spatial regions in the pattern of harmonic emission, with drastically different coherence properties (see Fig. 2.2). There was an inner region with the long coherence times described above and a diffuse outer halo, containing more than half of the total emitted flux, with an extremely short temporal coherence, of the order of just a few femtoseconds.

3.3 Some Insight into the Microscopic Generation Process

We unexpectedly found that this was one of the most direct proofs of the validity of the theoretical models currently used to describe the microscopic physical mechanisms involved in the process of HOH generation. According to the standard picture of the HOH generation process [14], during every half optical cycle of the laser pulse electrons undergo tunnel ionization through the potential barrier formed by the atomic potential and by the electric field potential of the laser; after being accelerated in the ionization continuum by the field, they may come back to the ion core and finally recombine to emit harmonic photons that release the accumulated kinetic and ionization energy. Single-atom models also predict that harmonics are emitted with an intensity-dependent phase, proportional to the amount of time spent in the continuum by the generating electrons.

Simple calculations show that the highest harmonic orders (in the so-called *cutoff*) can only derive from electrons which have been released at a well defined time in each half optical cycle of the laser. On the other hand, it is equally easy to see that lower-order harmonics (in the *plateau*) essentially come from two different classes of electrons which are emitted at different moments, spend different amounts of time in the continuum following different trajectories, but nevertheless come back to the ion with the same correct kinetic energy to generate that given harmonic (see Fig. 2.2). For these harmonics, the "short" trajectory imposes a phase that does not vary much with the laser intensity, whereas the phase corresponding to the "long" trajectory varies rapidly with the laser intensity. Such a "long" electronic trajectory gives rise to strongly divergent angular emission because the rapid spatial variation of the phase with the focused laser intensity leads to a strong curvature of the phase front. This radiation also has a very short coherence time, since the harmonic pulse is

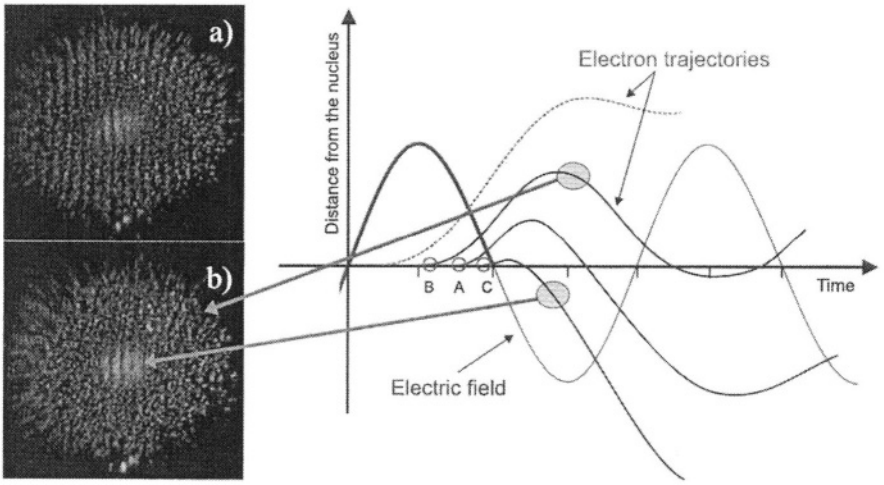

Figure 2.2. Snapshots of the interference fringes produced by the 15^{th} harmonic generated in argon. In a), taken at a delay of 0 fs, fringes appear all over the image with a good visibility, while they disappear in the outer region of b), taken at a delay of 15 fs. The diffuse halo surrounding the central bright spot has a much shorter coherence time than the inner region. On the right we show a schematic representation of the possible classic electronic trajectories leading to the emission of such harmonic photons every half laser optical cycle. Electrons which are ionized while the field amplitude grows are driven away from the ion and never recombine to generate harmonics (dashed curve). Electrons escaping with a decreasing field leave the ion, oscillate in the continuum and come back with additional kinetic energy that can be converted into photon energy (solid curves). The maximum return energy (corresponding to the highest harmonic orders generated) is carried by electrons ionized in **A**. A given lower harmonic (like the one on the left) can be generated by electrons released either in **B** or in **C**, since both trajectories correspond to the same final return velocity (same angle of intersection with the horizontal axis). Electrons "born" in **B** suffer a stronger intensity-dependent phase modulation since they spend a much longer time in the continuum.

strongly chirped due to the rapid temporal variation of the phase during the pulse. By contrast, the phase variation corresponding to the "short" trajectory is much less important: the emitted radiation has a long coherence time and is much more collimated (for a more detailed discussion see Ref. [15]). If one is somehow able to select just one of these electron trajectories, (for example, just using harmonics in the cut-off region, where XUV photons can only be generated by one electron trajectory corresponding to the maximum return kinetic energy), then HOH radiation will be essentially composed of a train of sub-femtosecond XUV pulses, emitted every half optical cycle of the driving laser pulse.

3.4 Collinear, Phase-Coherent, Harmonic Pulses

The experiments described above demonstrated that the process of HOH generation does not scramble the phase of the XUV radiation and that two phase-locked pump pulses can indeed produce two phase-locked harmonic pulses. In those experiments, however, the two harmonic pulses were generated in two spatially separated zones while, to generate the modulated spectrum described in Eq. 2.2, the pulses need to be collinear. This also means that the two time-delayed laser pulses have to interact with the same atoms to produce harmonics and that the second pulse of the pair may generate harmonics in a less efficient way or with significant phase disturbances due to the presence of free electrons. As a result, the possibility of using the produced harmonic pulses for some Fourier or Ramsey-type spectroscopy would be seriously compromised.

In order to check the phase lock in a collinear case, a new experiment was carried out in two different configurations [16]: in the first one, we selected a narrow wavelength interval and observed the temporal interference fringes as the time delay between the harmonic pulses was scanned; in the second, we observed the spectra corresponding to pairs of harmonic pulses at different time delays to confirm our results also from the spectral point of view, in a way similar to the experiments by Salières et al. [17].

The temporally integrated signal $I(\omega_s, \tau)$ observable at the exit slit of a spectrometer centred at ω_s as a function of the delay τ can be obtained by considering the harmonic field as the sum of two identical and temporally separated pulses. If $F(\omega - \omega_s)$ is the transmission function of the monochromator filter, which we assume to be symmetric and much narrower than the single-pulse spectrum $I_0(\omega)$, we obtain

$$I(\omega_s, \tau) \propto |I_0(\omega_s)\,(1 + \tilde{F}(\tau)\cos(\omega_s \tau)), \tag{2.5}$$

where $\tilde{F}(\tau)$ is the Fourier transform of $F(\omega)$, normalized to have $\tilde{F}(0) = 1$, and corresponds to the contrast of the resulting interference fringes. Measuring the fringe visibility as a function of the delay thus simply yields the Fourier transform of the filter transmission function. Expression 2.5 shows that two short time-delayed pulses that would not normally interfere due to their temporal separation may be forced to overlap again as a result of the broadening of their temporal profile introduced by the spectral filtering. The width of the spectral filter sets the maximum time delay for the existence of interference fringes[3]. In the case of identical harmonic pulses, there should be no degradation of the fringe contrast other than that caused by the limited spectral resolution of the monochromator and given by Eq. 2.5. If, on the other hand, one of the two harmonic pulses is degraded, for example, by passing through a partially depleted medium, then the fringe contrast should show a much faster decay with the time delay. The same effect is obtained not only in the case of a simple intensity imbalance, but also in the case of a phase disturbance of one of the two pulses.

The experimental set-up was similar to that of the previous experiment, and harmonics were observed downstream of the exit slit of the monochromator by means of a phosphor screen and a photomultiplier, while scanning either the time delay between the pulses or the monochromator wavelength. Figure 2.3 shows the fifth and seventh harmonic signals obtained by scanning the time delay on a small scale in the region of well-separated laser pulses. The stretching of the duration of the harmonic pulses due to the spectral filtering of the monochromator is evident, as these pulses keep interfering even for such large temporal separations. The same figure also presents the modulated two-pulse spectra corresponding to the same harmonics. According to expectations, the spectra exhibit the broad envelope of the single pulse, with a superposed sinusoidal modulation showing fringes with a period

$$\delta\lambda = \lambda^2/c\tau. \tag{2.6}$$

Our measurements were in good agreement with the simple expression 2.5, which only takes into account the finite spectral resolution of the monochromator, and is connected with the fact that, when the fringe period approaches such a value, the observed contrast starts to decrease due to the blurring of adjacent minima and maxima that finally washes out the whole interference pattern. It

[3]Note that, in the absence of such a filtering effect, interference fringes would only last for delays up to the coherence time of the pulses, of the order of a few tens of femtoseconds.

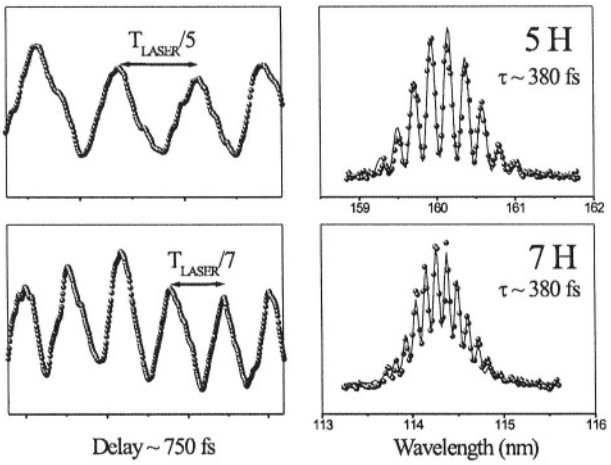

Figure 2.3. Two-pulse time-integrated intensity versus time delay for the fifth and the seventh harmonics at $\tau \approx 750$ fs (left column). Plots on the right show the two-pulse spectra of these harmonics at a fixed delay. The solid lines are fits to expression 2.5.

was thus demonstrated that no degradation of the fringe contrast was present due to the generation process itself (at least for medium-order harmonics and laser intensities up to 1.5×10^{14} W/cm^2) and that it was indeed possible to generate collinear pairs of phase-locked XUV radiation pulses. By replacing the filtering action of the monochromator with the narrow resonance of an atomic system, this technique may then allow the study of its spectral characteristics with an unprecedented resolution for this wavelength region.

3.5 Ramsey Spectroscopy with High-Order Harmonics

Ramsey-type spectroscopy with ultrashort laser pulses [18–20, 1]has been applied to bound state spectroscopy with optical sources in single-photon as well as in multi-photon and multi-step transitions [21, 2, 22, 23]. In its simplest scheme, one can consider the sinusoidally modulated two-pulse spectrum depicted in Fig. 2.1 b and imagine that a narrow atomic transition is placed somewhere under the broad spectral envelope. If the delay between the incoming pulses is varied, the fringe pattern moves and the transition will shift in and out of resonance in a sinusoidal fashion. Of course, when the delay gets so long that the period of the spectral fringes becomes comparable or smaller than the transition linewidth, then the contrast of the excitation modulation will tend to decay. From a different point of view, one can consider the first short pulse as inducing a coherence in the two-level system and creating a dynamical

polarization of the medium. The induced polarization oscillates at the transition frequency with a decaying amplitude during the dephasing time. The second pulse, depending on its phase with respect to the polarization oscillation, can enhance or destroy the residual system excitation. As a result, any excitation-related observable exhibits interference fringes when varying the delay between the two pulses. In more complex excitation schemes, involving more than two interacting states, the modulation of the fringe pattern and the appearance of beat notes can give information on the energy separation of nearby levels and on their lifetimes.

High-order harmonics are ideal candidates to study the spectral characteristics of high-lying excited states with one-photon transitions. With the experiments described above we had verified the possibility of producing collinear phase-locked harmonic pulse pairs so that the next step was to use them to perform high-resolution spectroscopy in the XUV. For the first test of Ramsey-type spectroscopy with HOH, a pair of krypton autoionizing states, resonant with the ninth harmonic of our Ti:sapphire laser, were chosen [24]. As schematically shown in the inset of Fig. 2.4, two phase-locked ninth-harmonic pulses at about 88 nm simultaneously excited the $4p^5(^2P_{1/2})6d'$ and $4p^5(^2P_{1/2})8s'$ states, separated by about 29 meV, well below the 90 meV of the single-pulse spectral width. The quantum interference of the states was expected to manifest itself as a fringe pattern in the electron signal versus the delay between the pulses, with a fringe spacing given by the atomic transition period [25], in this case about 0.29 fs. The modulation of the fringe contrast on the scale of the state lifetime, amounting to tens or hundreds of fs, should have reflected the decay and the possible beating of the autoionizing states.

The experimental set-up is sketched in Fig. 2.4 and was basically the same as used for the previous tests on phase coherence, but the exit slit of the monochromator was here replaced by a second pulsed gas jet of kripton atoms. An electron-energy and ion-mass time-of-flight spectrometer (TOF) was used to analyze the ionization products while scanning the inter-pulse time delay with a stepper-motor-controlled translation stage or with a piezoelectric crystal moving one arm of the interferometer. The electrons produced by the photoionization of krypton atoms left the interaction region and were analyzed by the TOF spectrometer, while the spectrally unresolved field of the selected harmonic was observed downstream from the interaction region by a phosphor/photomultiplier pair, whose signal gave a pulse-by-pulse monitor of the harmonic intensity. The interference fringes in the electron signal as the delay was smoothly varied around 110 fs are shown in Fig. 2.5. As the two states had an energy separation below the TOF electron-energy resolution, both continua

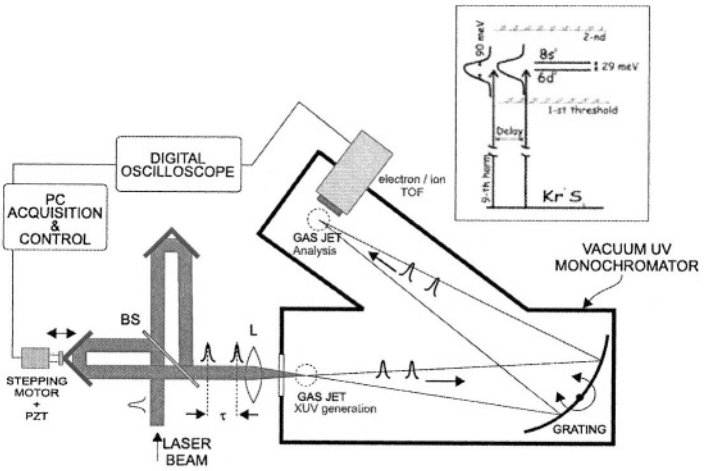

Figure 2.4. Experimental set-up and scheme of the interaction (inset), showing the involved autoionizing levels of the krypton atom: the ninth harmonic, generated by focusing the phase-locked pulse pair in the xenon jet, is selected by the monochromator grating and crosses the krypton jet in the interaction chamber. The electrons ejected in the one-photon ionization process are energy-analyzed by a TOF spectrometer

contributed to the observed ionization signal. The modulation was clearly visible above the statistical fluctuations, and had the expected period of about 290 attoseconds. The simultaneous detection of the transmitted harmonic intensity

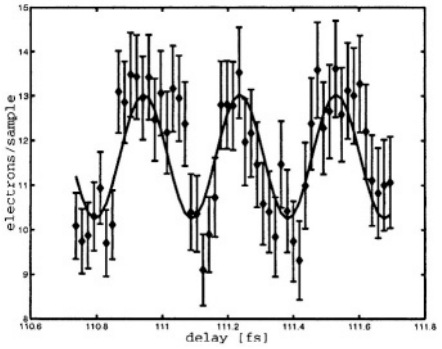

Figure 2.5. Detail of the fringe pattern around the 110 fs delay. The fringe spacing corresponds to the 0.29 fs period of the atomic transition.

did not show any modulation, thus verifying the absence of residual optical interferences between the harmonic pulses. The fringe contrast as a function of the pulse delay was compared with the theoretical curve obtained from the

state energies, widths, ionization constants, and the Fano parameters reported in the synchrotron measurements of Ref. [26]. Being in a perturbative regime, no coupling was taken into account between the two states, which thus evolve independently following two-state dynamics in the Fano approach. The theoretical ionization probabilities for the two states were then simply summed to give the total ionization signal. The energy difference between the two states was expected to give rise to a beating with a period of about 140 fs and our experimental data indeed showed such modulation in fairly good agreement with the calculated curve.

The clear signature of quantum interferences were the proof that a Ramsey-type approach in the XUV is possible. Such a spectroscopic tool, based on relatively simple table-top equipment, might thus become an attractive alternative to synchrotron radiation sources for selected applications. Furthermore, the use of more elaborate pulse sequences, or even the extension toward phase-locked harmonic pulse trains, might soon lead to the extension of the domain of precision spectroscopy and metrology (see the frequency-comb technique in Chapters 4 and 5 of this volume) to the short-wavelength region.

4. SUPERCONTINUUM

4.1 Basic Principles

Since the first observations in the late 1960s [27], the phenomenon of supercontinuum generation, i.e., the extreme spectral broadening resulting in the generation of white light when ultrashort and powerful laser pulses propagate in a transparent medium, has been demonstrated in a variety of materials, including solids, liquids [28], and gases [29, 30]. Its broadband and ultrashort characteristics make it a unique light source [31, 32]for applications, and it is now routinely used for femtosecond time-resolved spectroscopy [30, 33], in optical pulse compression for the generation of ultrashort pulses [34, 35], or as a seed pulse of optical parametric amplifiers [36–38].

Supercontinuum (SC) generation results from a complex interplay of self-phase-modulation [27, 28, 39], self-focusing [29, 40], and several other nonlinear optical effects. The collapse of the beam profile due to self-focusing is one of the main ingredients for the generation of the continuum when the power of the pump pulse reaches a critical threshold. Experiments have indeed shown that the threshold for SC generation corresponds to the calculated critical value for self-focusing [29, 30, 40, 41]. It has been demonstrated that when intense ultrashort laser pulses are focused in transparent media, they tend to break up into a number of intense filaments [42–44], and that, due to the competition

between focusing by the Kerr effect and defocusing by free electrons (created in multiphoton or avalanche ionization), the diameter of these filaments and the peak laser intensity inside them tends to remain constant against increasing input pulse energies [45].

The combined action of the highly nonlinear phenomena involved in the generation of SC might lead one to conclude that even small perturbations in the conditions of interaction with the medium can strongly affect the amplitude and phase properties of the white-light pulses. In particular, one may expect that small intensity variations in the pump pulses or small inhomogeneities in the materials may lead to dramatic phase and intensity fluctuations in the generated supercontinua.

4.2 Phase Preservation in the Supercontinuum Generation Process

After the experiments on the coherence of high-order harmonics, we decided to use the same simple experimental apparatus to test the mutual phase coherence of the light pulses generated in this different kind of extremely nonlinear process. We just replaced the system for harmonic generation with a plain 2 mm thick plate of calciumfluoride (CaF_2) after the misaligned Michelson interferometer, so that the two phase-locked laser pulses could independently produce two white-light pulses. After the interaction zone and after the two diverging continua had propagated in air for some distance, they were finally overlapped on a screen where we hoped to observe interference fringes.

The results of this simple experiment were once again quite unexpected: when the two pump pulses were properly balanced in intensity and adjusted for zero relative delay, the two white-light continua that had been separately generated showed the surprisingly clear and stable white interference fringes depicted in Fig. 2.6, indicating that we were dealing with highly phase-correlated secondary sources[4] [46].

In order not to damage the medium, the pulse energy was limited to about 1 μJ, and the generation of a white-light continuum was normally observed to proceed through the creation of a single light filament with an estimated peak intensity of the order of 10^{12-13} W/cm^2. Higher energies involved the

[4]Note that there is a substantial difference between this and a simple Young's or Michelson's type experiment: in such cases two spatial portions of the same beam, or two time-delayed replicas of the same pulse, are recombined to give interference. In our experiments on HOH and SC, on the contrary, the interference fringes appear because of the spatio-temporal superposition of two secondary light pulses independently generated in two separate positions of the medium. For the complex and apparently unpredictable characteristics of the generation processes at play, one could expect such pulses to be highly unrelated.

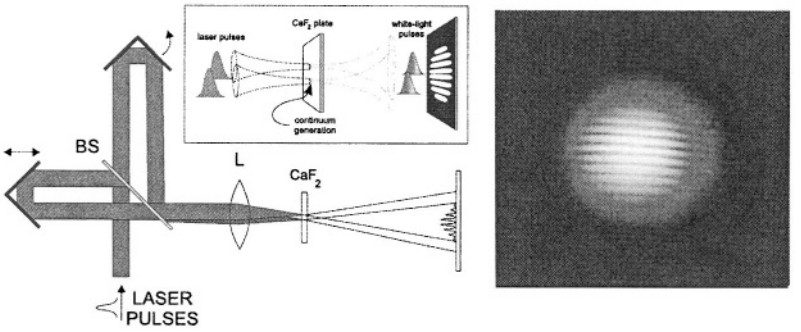

Figure 2.6. Scheme of the experiment for the observation of white-light interference fringes. The two pump pulses are generated by the same laser system and by the same Michelson interferometer described above. Two independent SC pulses are generated in the material and then propagate and overlap on a screen. A snap-shot of the observed interference pattern is also shown, taken with an exposure time of about 2 seconds and with a laser repetition rate of 1 kHz. The very good visibility of the fringes indicates that the phase lock is not only preserved on a shot-to-shot basis, but that a constant phase relationship is maintained over at least thousands of shots.

breakup of the pulse into multiple filaments, giving rise to highly structured patterns as a result of the spatial interference among the different, and mutually coherent, white-light sources thus produced. Although visually interesting, we tried to avoid this effect, and all the measurements were performed in the single-filament regime. In general, any transparent material available in the laboratory (from quartz and glass plates to water cells and Plexiglas windows) was able to produce nicely interfering white light at various degrees of efficiency.

4.3 Collinear, Phase-Coherent, Supercontinuum Pulses

The previous experiment, dealing with the mutual coherence of SC pulses generated with amplified laser systems in bulk media, demonstrated that spatially separated white-light sources could exhibit high-visibility spatial interference fringes [46–48]. However, no indication had been given about the possibility of generating collinear phase-locked continua in a bulk medium. Although this is the fundamental process at the base of the recent and successful technique of frequency comb generation in photonic fibers with mode-locked lasers (see Sect. 6), the equivalent mechanism in bulk media has to take place at much higher intensities and the nonlinear processes involved are therefore far less smooth and controllable. In the previous case of spatially separated sources, the pump laser pulses did not interfere in the medium and each pulse generated white light independently from the other. In the collinear case, a sub-

stantial optical interference can take place between the laser pulses for delays shorter than the pump coherence time and the high intensities reached at the interference maxima may damage the material and prevent stable and efficient generation. Even in the case of delays longer than the temporal coherence of the pump pulses, the second pulse of the white-light pair has to be generated in a region which has already strongly interacted with the first one, and one might expect a degradation of the mutual coherence of the two supercontinua.

The next step was then to set up an experiment to investigate the coherence properties of time-delayed and phase-locked collinear SC pulses [49]. By mounting one of the interferometer mirrors on a PZT-controlled tilt stage, one could accurately split and recombine the 30 fs laser pulses to make them propagate collinearly and produce clear spectral interferences when time-delayed. A lens focused the pulses in glass windows with thickness ranging between 0.5 and 5 mm and the spectra of the produced white light were observed after a re-collimating lens by means of a spectrometer, based on a 2048-pixel photodiode array and with a spectral coverage extending from 520 to about 1180 nm. In the ideal case, where the two time-delayed white-light pulses are perfectly phase-locked, their combined spectrum is easily found from Eq. 2.2 and is expected to show a clear sinusoidal modulation of high visibility, with a period depending on the inter-pulse delay and on the wavelength (see Eq. 2.6). Our objective was then to verify that, when the two white-light pulses were generated by two time-delayed, phase-locked laser pulses with reasonably equal efficiencies, such a modulated spectrum would indeed appear and extend over all the visible and near-IR regions. Figure 2.7 shows the appearance of

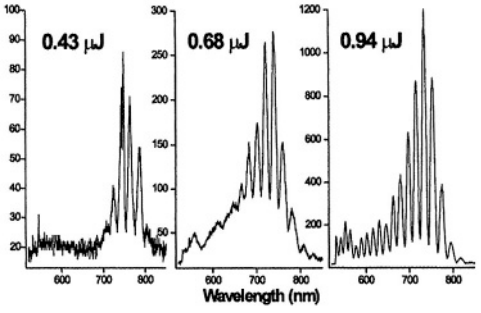

Figure 2.7. Appearance of white-light spectral interference fringes on the visible side of the laser spectrum in a 1 mm thick glass plate. In the sequence of spectra measured at different single-pulse energies, one can observe the birth of a single supercontinuum pulse and the appearance of the second, phase-locked pulse, which produces a clear sinusoidal modulation in the spectrum.

the white-light continuum on the short-wavelength side of the modulated laser

spectrum: at low power, no SC was present, but when the pulse energy was increased, visible components started to appear without visible modulations. Only when the pulse energy was increased close to 1 μJ, clear spectral interferences appeared. This is simply explained by the presence of a threshold behavior connected with the modifications in the spatial profile of the pulses due to self-focusing, combined with a slight imbalance in the peak intensity of the two pump pulses. While at low power neither pulse had suffered sufficient self-phase-modulation to significantly broaden its spectrum, at intermediate values one of the two had reached the critical power for self-trapping and the intensity in the so-formed filament had given rise to the new spectral components in the visible region. Only when the second pulse reached the same threshold, a comparable amount of white light was suddenly coherently generated, allowing the corresponding spectral components of the two pulses to interfere. By recording the evolution of the different spectral components of the SC in the single-pulse and single-filament regime as a function of the laser pulse energy we indeed found a general behavior similar to the one shown in Fig. 2.8 for the region around 550 nm. Experimental values in the 5-10 MW range for the threshold power of supercontinuum formation agree well with the calculated critical power for the onset of self-focusing and indicate the close connection between the two phenomena. As long as the pulse energy was not increased

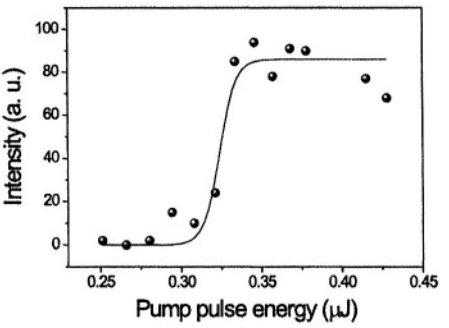

Figure 2.8. Behavior of the SC intensity variation as a function of the incoming laser pulse energy for a wavelength of about 550 nm. Filled circles are experimental data while the solid line is a fit with an hyperbolic tangent function.

too much above this single-filament threshold, to a level such that both pulses were able to independently generate stable white light, the resulting spectrum was always characterized by very stable interference fringes of high contrast extending through all the visible and up to about 1.1 μm. The pulse peak intensity in the focus under these conditions was estimated to range between 1 and

5 times 10^{12} W/cm^2 depending on the medium thickness, with a waist radius of about 15 μm.

By changing the delay τ between the pump pulses it was possible to vary the period of the spectral fringes. Two examples of the spectra, in the visible and in the near-IR region, corresponding to different time delays between the pulses, are shown in Fig. 2.9. The fringe period measured in the region around

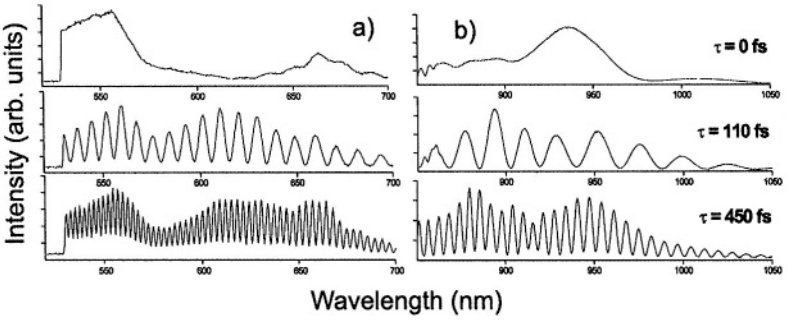

Figure 2.9. Visible a) and near-IR b) portions of the two-pulse SC spectrum displaying sinusoidal modulations of different period as a function of the time delay between the pump pulses.

900 nm is also shown in Fig. 2.10 as a function of the delay. The expected behavior (see Eq. 2.6) with the inverse of the time separation between the pump pulses is well reproduced by the experimental data. Increasing the time

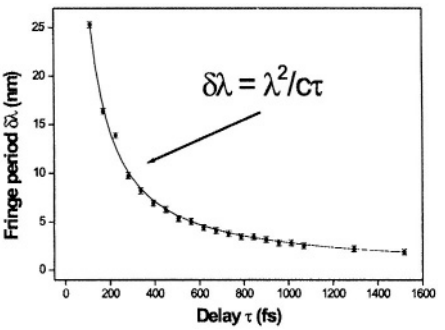

Figure 2.10. Fringe period as a function of the time delay τ between two laser pulses. Filled circles represent data points while the solid curve is a fit to the expected $1/\tau$ behavior.

delay normally reduces the fringe visibility due to the finite resolution of the spectrometer. However, other sources of contrast degradation may result from a difference in the conversion efficiency of the two laser pulses or the loss of mutual coherence between the two supercontinua. If the first pulse somehow

degrades the medium after its passage, then the second pulse generates much less intense white light and the fringe contrast $V(r)$ decreases as

$$V(r) = \frac{2\sqrt{r}}{1+r}, \tag{2.7}$$

where $r = I_1(\omega)/I_2(\omega)$ is the ratio of the two SC intensities. Even without any intensity imbalance between the two white-light pulses, the passage of the first pulse might perturb the phase evolution of the second and contribute to a decrease of the fringe contrast. In order to discriminate between these sources of contrast decay, we studied the behavior of the fringe visibility as a function of the relative pulse delay for different spectral components. In particular, we determined the decay curves for two regions of the white-light spectrum above and below the laser wavelength, and compared them with the visibility curve for the modulated laser spectrum obtained without interaction with the medium. Once again, we were able to show that the fringe contrast nicely followed the decay curve as expected in the case of purely resolution-limited visibility, and that SC generation does not spoil the phase coherence of the laser pulses.

Finally, we tested the effects of pulse energy imbalance on the generation and the phase coherence of the white light. As one could expect from Fig. 2.8, we found that, above the threshold and close to the balanced condition, SC can stand as much as 30% of pump intensity imbalance without substantially degrading the fringe contrast (see Fig. 2.11). On the contrary, the change in

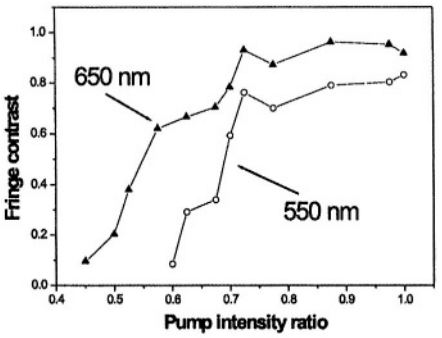

Figure 2.11. Fringe contrast as a function of the pump pulse energy imbalance for two spectral regions of the SC: triangles correspond to 650 nm and circles to 550 nm. Solid lines connecting the experimental points are just a guide for the eye.

the intensity of one beam produced noticeable effects in the position of the fringes. A pulse peak intensity increase ΔI of about 3×10^{12} W/cm^2 in the

focus caused a shift of about 6 fringes in the spectral interference pattern around 600 nm. This fringe shift could be compensated by increasing the path length of the other pulse, consistent with the effects of a positive nonlinear refraction index n_2. One could easily verify that this fringe shift is compatible with the one calculated from

$$\Delta\varphi = \frac{2\pi}{\lambda} n_2 \Delta I L \tag{2.8}$$

for the propagation in a medium of thickness $L \approx 5$ mm and nonlinear refractive index $n_2 \approx 10^{-16}$ cm^2/W in the case of a similar intensity variation.

4.4 Multiple-Beam Interference from an Array of Supercontinuum Sources: a Spatial Comb

As a further step to test the mutual coherence of SC, we realized the spatial-domain counterpart of the frequency-comb configuration, by generating a linear array of equally spaced SC sources in a bulk material and studying their far-field interferences[5] [50].

The usual Michelson interferometer was used in a slightly different configuration: by properly adjusting the angle of one of its folding mirrors, it was possible to change the angle between the outgoing laser pulses and produce straight interference fringes of variable period in the zone of beam crossing. A cylindrical lens was then placed after the interferometer in order to focus the outgoing pulses along a direction orthogonal to the plane containing the laser beams. In such a configuration the straight interference fringes were compressed down to between 10 and 20 microns in one dimension, while the spacing and the width of the spots in the other dimension could be simply adjusted by changing the relative angle between the two beams. Glass and quartz plates of different thickness (ranging from 2 to 10 mm) were placed in the focus position, and the regions of high intensity corresponding to the maxima of the interference fringe pattern could become the sources for SC emission. The laser pulse energy was varied in order to reach the threshold for white light generation from several consecutive interference maxima. Even at the highest intensities available with our laser system, SC generation from the different sources in the array always proceeded through the formation of a single filament, and multiple filamentation from a single source was never observed. After the interaction region, the SC pulses propagated towards a screen where they formed complex interference patterns. The fringe system was studied by scanning a photomul-

[5]Note that multiple Supercontinuum sources require an even more stringent relative-phase stability in order to produce a stable and clear interference pattern.

tiplier, apertured by a pinhole, along a direction perpendicular to the fringes by means of a computer-controlled translation stage, while colored filters were placed in front of the detector to select different spectral regions in the visible continuum. In order to study the near-field region inside the transparent material, the source area was also imaged on a distant screen and magnified (by a factor of about 40) by means of a lens. The interaction geometry is illustrated

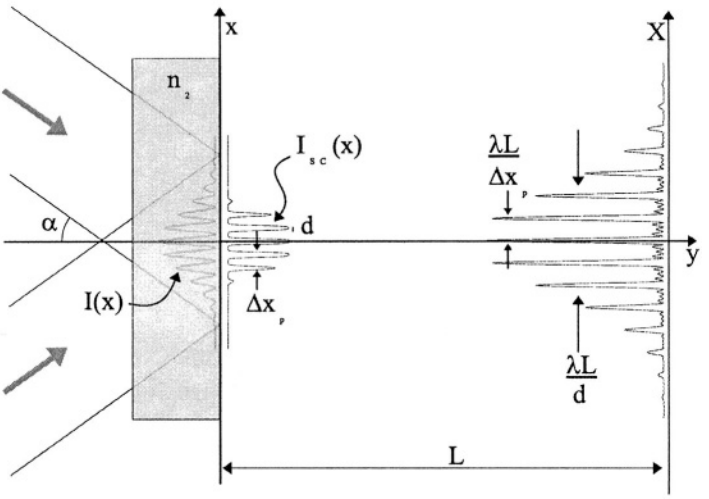

Figure 2.12. Sketch of the experimental set-up illustrating the geometry of the interaction. Two laser pulses intersect at an angle 2α and form an interference pattern on the x plane inside the material. The maxima of this interference pattern become the sources for supercontinuum radiation which propagates to a screen placed at a distance L.

in Fig. 2.12: the two laser beams intersect with an angle 2α and we assume that the delay between the two arms of the interferometer is adjusted so that the pulses cross the plane $x = 0$ at the same time. In this case, the different positions along the x axis simply map different relative delays τ between the arrival time of the two pulses as

$$\tau(x) = 2\frac{x}{c}\sin(\alpha). \tag{2.9}$$

If the coherence time of the laser pulses is τ_c (we assume that we are dealing with Fourier-transform-limited Gaussian pulses, with a pulse duration $\tau_c \approx 30$ fs and peak intensity I) then one can expect to observe an interference fringe

pattern of good visibility for a spatial extension of about

$$\Delta x_c \simeq \frac{c\tau_c}{2\sin(\alpha)} \tag{2.10}$$

and with a fringe period of

$$\Delta x_p = \frac{\lambda}{2\sin(\alpha)}. \tag{2.11}$$

So, by varying the angle α it is easily possible to change the dimensions of the source area and the fringe spacing in a wide interval (note that, in all cases, the total number of fringes in the array is constant, independent of the angle between the beam directions, and of the order of 10-20). Neglecting the spatial distribution of the pump intensity and considering a simple interference of two plane waves, the two-pulse pump intensity distribution $I(x)$ in the $y = 0$ plane can be simply found. In this case

$$I(\tau) = 2I(1 + V(\tau)\cos(\omega\tau)), \tag{2.12}$$

where the fringe visibility $V(\tau)$ is given by

$$V(\tau) = e^{-(\frac{\tau}{\tau_c})^2 \ln 2} \tag{2.13}$$

and one can make use of Eq. 2.9 to convert the time delays into a transverse spatial position.

In order to simulate the process of white-light generation in the case of our multiple-source arrangement, we modeled the SC intensity dependence on the pump intensity with a hyperbolic tangent function, according to the behavior observed in Fig. 2.8[6]. Clearly, also the number N of SC sources (and, consequently, the spatial extension of the array) is a directly controllable parameter, via the control of the pump pulse energy. High laser power allows generation from many spatially-separated sources, while a lower power limits the production of white light to only a few central interference maxima. By varying the pump pulse energy, the number of SC sources was changed from 3-4 to as many as 40 when the full laser power allowed self-focusing also for interference maxima in the extreme wings of the pattern. Figure 2.13 shows

[6]Note that the introduction of an hyperbolic tangent function with a characteristic threshold and saturation behavior has an evident connection with the onset of beam self-focusing and with the sudden intensity clamping due to the formation of a filament in the medium.

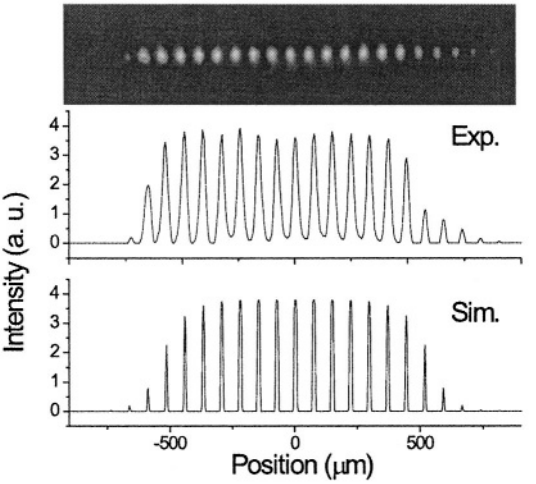

Figure 2.13. Experimental CCD image of the SC array source region. Also shown are the profiles obtained by an horizontal cut across the image (middle plot) and the simulated SC intensity distribution from Eqs. 2.12 and 2.13 (bottom plot). An array of about 15 white-light sources of almost constant intensity was produced in this case: the extension of the array was measured to be about 1 mm, with an inter-source spacing of 75 μm.

a near-field image, taken with a CCD camera, of the interaction region, where many equally-spaced sources of white light were clearly visible. An horizontal cut of this figure indicated that the central part of the pump interference pattern produced SC secondary sources of almost constant intensity despite the Gaussian profile of $I(x)$. The use of the hyperbolic tangent function to cut the low-intensity pump regions and to saturate the interference maxima made it possible to reproduce the intensity distribution of the white-light sources in a very reasonable way.

In order to evaluate the mutual phase coherence among the white-light sources, we studied the far-field interference patterns produced by the array on a screen placed at a distance *L*. As indicated in Eq. 2.3, a linear array of *N* phase-locked, infinitesimal sources equally spaced by a distance Δx_p should produce an array of intense sharp peaks spaced by $\frac{\lambda L}{\Delta x_p}$, with $N-2$ smaller (by a factor of approximately N^2) peaks interposed (see Fig. 2.12 for reference). Figure 2.14 a shows the experimental profile of the interference pattern produced by the array of white-light sources as seen by a scanning detector in the far-field. The expected structure described by Eq. 2.3 is evident, with a clear array of strong interference maxima with smaller peaks interposed at regular distances. In this particular case, the laser pulse energy had been adjusted so

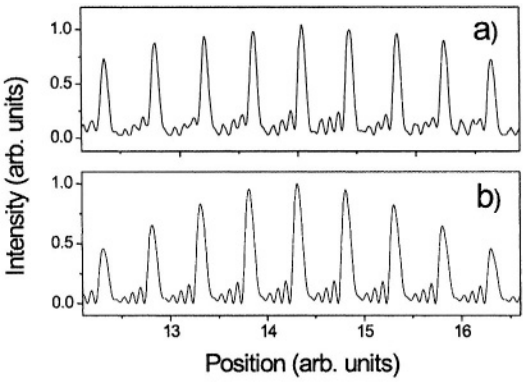

Figure 2.14. a) Experimental profile of the multiple-SC-beam interference pattern detected by scanning a photomultiplier in the far-field. Only the green part of the spectrum is selected by means of colored filters. b) Calculation of the far-field interference pattern generated by an array of phase-locked SC sources under the same conditions as a). A relative phase, proportional to the laser intensity in the different filaments, is introduced in order to reproduce the experimental behavior of the secondary peaks.

that only 6 to 8 interference maxima reached the threshold intensity for SC generation and we could infer that the white-light sources were filaments with a diameter of the order of $10\ \mu\mathrm{m}$ or less. Although the intensity distribution among the secondary maxima was not as regular as expected from the ideal case, it was nevertheless clear that only a smooth and slowly varying phase had to be present across the array of SC sources. By using the calculated intensity distribution in the source area and the expression 2.8 for the induced nonlinear phase, we could simply estimate the phase distribution $\Delta\varphi(x)$ in the array, and find that a propagation distance of a few mm was sufficient to establish phase shifts of tens of radians between the central peaks and the outer ones. A simulated far-field pattern, obtained by Fast Fourier Transformation of the calculated source intensity-phase distributions, is shown in Fig. 2.14 b for the situation corresponding to the experimental results of Fig. 2.14 a. The qualitative agreement with the experimental data is evident.

Also, in this case, we found that all the multiple-beam interference patterns were extremely stable in time, indicating that the phase distribution was essentially the same from shot to shot, with little perturbation due to laser intensity fluctuations.

5. PHASE PRESERVATION IN CHIRPED-PULSE AMPLIFICATION

One further test concerning the phase preservation of ultrashort radiation involved the process of chirped-pulse amplification, normally used to boost the energy of the pulses coming from a mode-locked laser [51]. Here the idea was to compare, in an interferometric (i.e., phase-sensitive) way, a single pulse from a laser oscillator with its replica having undergone the process of amplification, to determine if their phases had been significantly scrambled or not[7]. By placing a beamsplitter before the pulse stretcher of the laser amplifier, both the oscillator pulses and their amplified versions were emitted from the system and made to interfere, after the delay in the multipass amplifier had been exactly compensated by an external delay line. Temporal interferences between a single amplified pulse and its twin in the oscillator train (at 80 MHz repetition rate) were observed as periodic modulations of their combined signal while finely scanning the optical delay line. Measurements were performed for different numbers of passes in the amplifier and for varying gain factors, up to full amplification and re-compression of 0.6 mJ pulses.

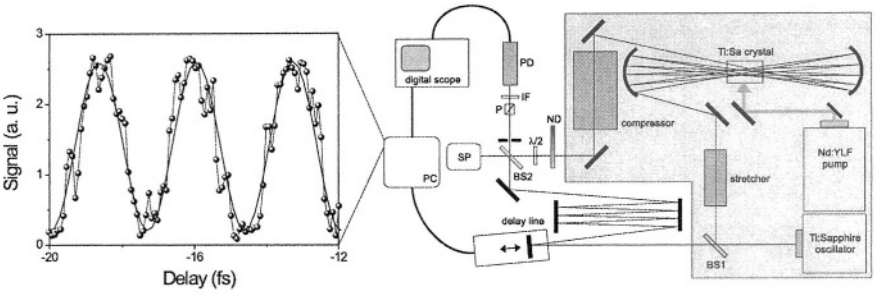

Figure 2.15. Experimental set-up. The shaded area delineates the amplified laser source. ND: variable neutral density filter; P: cube polarizer; $\lambda/2$: half-wave plate; IF: narrow-band interference filter; PD: fast photodiode; SP: spectrometer; BS1 and BS2: 50% beam splitters; PC: personal computer. Also shown is the interference signal (filled circles) obtained while scanning the delay between the original laser pulse and its amplified replica. The solid line is a fit to a sine function.

In order to single out the possible deleterious effects of amplification from those coming from other unavoidable instabilities in the system on the phase co-

[7]Possible causes of dephasing include cross-phase modulations due to a pulse-to-pulse jitter of the pump energy or self-phase modulations due to shot-to-shot variations in the intensity of the amplified pulse itself or, finally, beam-pointing instabilities in the stretcher/compressor stages of the amplifier.

herence of the CPA pulses, we compared all the measurements of the oscillator-amplifier first-order cross-correlations with the same signals obtained with the amplification turned off. Figure 2.15 shows the experimental set-up and a portion of the cross-correlation signal obtained after nine passes in the amplifier. Clear and stable interference fringes demonstrated that the effect of amplification was reproducible and could in principle be controlled. Even in the case of full amplification and re-compression, the measured r.m.s. phase jitter between the two pulses was about 0.4 rad and did not change, within the accuracy of the measurement procedure, while switching on and off the pump laser (thus indicating that its main cause was environmental noise and not amplification). A prudential assumption of 0.1 rad as the upper limit for the total r.m.s. amplification-induced phase jitter was thus established and allowed one to conclude that the CPA process can substantially preserve the phase fingerprints of the original pulses.

6. FREQUENCY COMBS, ABSOLUTE PHASE CONTROL, AND ATTOSECOND PULSES

Besides their interest for a better understanding of the basic mechanisms and for the applications of these novel "extreme" sources, the experiments on the coherence properties in HOH and SC generation and CPA were fundamental starting points for the successive developments in the field of optical metrology and attophysics.

The measurements on the phase coherence of HOH had demonstrated that just a few main electronic trajectories are responsible for the XUV emission and that, by properly selecting the experimental conditions, it is possible to select only one of such trajectories and thus emit a single XUV attosecond pulse for each half-cycle of the pump laser. If an intense laser pulse with a duration of just a few optical cycles (i.e., less than about 5 fs for a visible/near-IR pulse) is used to generate harmonics, and its intensity is selected such that cut-off photons can be generated only close to the peak of the pulse envelope, then the emitted radiation will consist of at most one or two attosecond-duration bunches of XUV photons. However, the emission pattern will normally not be repetitive from one laser shot to another, making the diagnostics and the use of such isolated attosecond pulses almost impossible, because, when dealing with few-cycle laser pulses, another parameter (normally forgotten for pulses of longer duration) comes into play and becomes crucial. This parameter is the so-called carrier-envelope-offset phase φ_{CEO}, and its variation in mode-locked laser pulses is connected with the fact that the phase velocity and group velocity inside the laser cavity are different. The absolute phase of the carrier

field oscillation thus normally slips by $\Delta\varphi_{CEO}$ with respect to the envelope from one pulse to the next one in a mode-locked train. In order to generate single attosecond pulses in a stable and reproducible way, one needs to start from identical and phase-customizable few-cycle pump pulses, and the only possibility to achieve this is by controlling and stabilizing φ_{CEO}.

This is where our activity on the supercontinuum came into play: by demonstrating the phase preservation in the process of SC generation, we had also shown that it was in principle possible to build a white-light frequency comb using a mode-locked laser to produce a train of phase-locked SC pulses after the interaction with a nonlinear medium. The results of our experiments and the introduction of a new kind of special optical fiber[8] [52]contributed to make such devices a reality and to revolutionize the whole field of optical metrology and spectroscopy [53–56]. Femtosecond frequency combs are now replacing old-style frequency chains wherever a precise measurement of an optical frequency is required because, with the realization of combs so wide as to extend over more than one optical octave, this technique now constitutes a solid self-referencing method, allowing the measurement of absolute optical frequencies with extreme accuracy in a single step from the microwave frequency standard [56]. Indeed, the frequency of the n^{th} mode of the comb is simply given by

$$f_n = nf_r + f_0, \tag{2.14}$$

where f_r is the easily measured and controlled laser repetition rate, and f_0 is the so-called *offset frequency,* which can be measured by beating the blue side of an octave-spanning comb with the red side of its frequency-doubled version. The interesting part is that f_0 is simply related to $\Delta\varphi_{CEO}$ by

$$f_0 = \frac{\Delta\varphi_{CEO}\, f_r}{2\pi} \tag{2.15}$$

i.e., f_0 is just a measure of the slip rate of φ_{CEO}. It is evident that, by setting f_0 to zero or appropriately stabilizing it by some feedback loop, it becomes possible to control the absolute phase of the laser field and to generate a sequence of truly identical pulses. Finally, the demonstration that the phase characteristics

[8] "Photonic crystal fibers" or "holey fibers", essentially consisting of a very small silica core surrounded by a regular structure of "holes". They have the interesting characteristic of supporting the propagation of highly spatio-temporally confined visible pulses over long distances. This allows high nonlinearities to build up along the fiber and can give rise to SC generation already from nanoJoule-level pump pulses of a mode-locked laser.

of low-energy pulses from a mode-locked laser can be preserved in the process of chirped-pulse amplification [51], has now paved the way for the routine production of few-cycle, high-intensity, and phase-controlled, pulses.

Such pulses have already proved capable of generating reproducible single attosecond pulses for extremely high temporal resolution studies [57], but the availability of phase-controlled intense pulses will also have strong implications for a whole range of new phenomena in high-intensity laser-matter interactions, where the absolute phase of the field plays a fundamental role to trace [58]and steer [57, 59–61]the electronic dynamics in unprecedented ways.

7. CONCLUSIONS

We have reported some recent experiments aimed to demonstrate and characterize the coherence properties of two kinds of "extreme" radiation sources: high-order laser harmonics and supercontinuum. Besides allowing the first applications of XUV interferometry and Ramsey spectroscopy, the studies on HOH generation have shed light on the basic mechanisms involving the role of electronic trajectories in the production of high-energy photons. On the other hand, experiments on the phase coherence in SC generation started the adventure of femtosecond frequency combs that, besides their fundamental role in precision spectroscopy and metrology, are now allowing the control of the absolute phase of few-cycle pulses. These two fields are now converging in a new, exciting direction – the generation and application of the shortest pulses ever created.

Acknowledgments

Most of the above experiments were performed at LENS and all these results were the successful combination of the skills of many invaluable collaborators (the list is too long to thank all of them here) and of the inspiring discussions with Ted Hänsch.

References

1. M. Bellini, A. Bartoli and T. W. Hänsch, *Opt. Lett.* **22**, 540 (1997).
2. V. Blanchet, C. Nicole, M. A. Bouchene and B. Girard, *Phys. Rev. Lett.* **78**, 2716 (1997).
3. J. N. Eckstein, A. I. Ferguson and T. W. Hänsch, *Phys. Rev. Lett.* **40,** 847 (1978).
4. M. Ferray, A. L'Huillier, X. F. Li, L. A. Lompré, G. Mainfray and C. Manus, *J. Phys. B* **21**, L31 (1988).
5. A. McPherson, G. Gibson, H. Jara, U. Johann, T. S. Luk, I. McIntyre, K. Boyer and C. K. Rhodes, *J. Opt. Soc. Am. B* **4**, 595 (1987).

6. P. Saliéres, A. L'Huillier, P. Antoine and M. Lewenstein, *Adv. At. Mol. Opt. Phys.* **41**, 83 (1999).

7. C. Lyngå, F. Ossler, T. Metz and J. Larsson, *Appl. Phys. B* **72**, 913 (2001).

8. K. S. E. Eikema, W. Ubachs, W. Vassen and W. Hogervorst, *Phys. Rev. A* **55**, 1866 (1997).

9. F. Brandi, D. Neshev and W. Ubachs, *Phys. Rev. Lett.* **91**, 163901 (2003).

10. M. Bellini and T. W. Hänsch, *Appl. Phys. B* **65**, 677 (1997).

11. R. Zerne, C. Altucci, M. Bellini, M. B. Gaarde, T. W. Hänsch, A. L'Huillier, C. Lyngå and C. G. Wahlström, *Phys. Rev. Lett.* **79**, 1006 (1997).

12. D. Descamps, C. Lyngå, J. Norin, A. L'Huillier, C.-G. Wahlström, J.-F. Hergott, H. Merdji, P. Saliéres, M. Bellini and T. W. Hänsch, *Opt. Lett.* **25**, 135 (2000).

13. M. Bellini, C. Lyngå, A. Tozzi, M. B. Gaarde, T. W. Hänsch, A. L'Huillier and C.-G. Wahlström, *Phys. Rev. Lett.* **81**, 297 (1998).

14. P. B. Corkum, *Phys. Rev. Lett.* **71**, 1994 (1993).

15. C. Lyngå, M. B. Gaarde, C. Delfin, M. Bellini, T. W. Hänsch, A. L'Huillier and C.-G. Wahlström, *Phys. Rev. A* **60,** 4823 (1999).

16. M. Bellini, C. Cavalieri, C. Corsi and M. Materazzi, *Opt. Lett.* **26**, 1010 (2001).

17. P. Saliéres, P. L. Le Deroff, T. Auguste, P. Monot, P. D'Oliveira, D. Campo, J. F. Hergott, H. Merdji and B. Carré, *Phys. Rev. Lett.* **83**, 5483 (1999).

18. M. M. Salour, *Rev. Mod. Phys.* **50**, 667 (1978).

19. J. T. Fourkas, W. L. Wilson, G. Wakerle, A. D. Frost and M. D. Fayer, *J. Opt. Soc. Am.* **6,** 1905 (1989).

20. R. R. Jones, D. W. Schumaker, T. F. Gallagher and P. H. Bucksbaum, *J. Phys. B* **28**, L405 (1995).

21. R. Van Leeuwen, M. L. Bajema and R. R. Jones, *Phys. Rev. Lett.* **82**, 2852 (1999).

22. M. A. Bouchene, V. Blanchet, C. Nicole, N. Melikechi, B. Girard, H. Ruppe, S. Rutz, E. Schreiber and L. Wöste, *Eur. Phys. J. D* **2**, 131 (1998).

23. M. A. Bouchene, C. Nicole and B. Girard, *Opt. Commun.* **181**, 327 (2000).

24. S. Cavalieri, R. Eramo, M. Materazzi, C. Corsi and M. Bellini, *Phys. Rev. Lett.* **89**, 133002 (2002).

25. S. Cavalieri and R. Eramo. *Phys. Rev. A* **58**, R4263 (1998),

26. J. Z. Wu, S. B. Whitfield, C. D. Denise Caldwell, M. O. Krause, P. Van Der Meulen and A. Fahlman, *Phys. Rev. A* **42,** 1350 (1990).

27. R. R. Alfano and S. L. Shapiro, *Phys. Rev. Lett.* **24,** 584 (1970).

28. R. L. Fork, C. V. Shank, C. Hirlimann and R. Yen, *Opt. Lett.* **8,** 1 (1983).

29. P. B. Corkum, C. Rolland and T. Srinivasan-Rao, *Phys. Rev. Lett.* **57,** 2268 (1986).

30. F. A. Ilkov, L. Sh. Ilkova and S. L. Chin, *Opt. Lett.* **18,** 681 (1993).

31. R. R. Alfano. *The Supercontinuum Laser Source,* Springer-Verlag, New York, 1989.

32. "Special Issue on Supercontinuum", *Appl. Phys. B* **77** (2003).

33. S. A. Kovalenko, A. L. Dobryakov, J. Ruthmann and N. P. Ernsting, *Phys. Rev. A* **59**, 2369 (1999).

34. R. L. Fork, C. H. Brito Cruz, P. C. Becker and C. V. Shank, *Opt. Lett.* **12,** 483 (1987).

35. E. T. J. Nibbering, O. Dühr and G. Korn, *Opt. Lett.* **22,** 1335 (1997).

36. V. V. Yakovlev, B. Kohler and K. R. Wilson, *Opt. Lett.* **19,** 2000 (1994).

37. M. K. Reed, M. K. Steiner-Shepard and D. K. Negus, *Opt. Lett.* **19,** 1885 (1994).

38. K. R. Wilson and V. V. Yakovlev, *J. Opt. Soc. Am B* **14**,444 (1997).

39. G. Y. Yang and Y. R. Shen, *Opt. Lett.* **9**, 510 (1984).

40. W. L. Smith, P. Liu and N. Bloembergen, *Phys. Rev. A* **15**, 2396 (1977).

41. J. Ranka, R. W. Schirmer and A. Gaeta, *Phys. Rev. Lett.* **77**, 3783 (1996).

42. A. Brodeur, F. A. Ilkov and S. L. Chin, *Opt. Commun.* **129,** 193 (1996).

43. A. Brodeur and S. L. Chin, *Phys. Rev. Lett.* **80**, 4406 (1998).

44. A. Brodeur and S. L. Chin, *J. Opt. Soc. Am. B* **16,** 637 (1999).

45. W. Liu, S. Petit, A. Becker, N. Aközbek, C. M. Bowden and S. L. Chin, *Opt. Commun.* **202**, 189 (2002).

46. M. Bellini and T. W. Hänsch, *Opt. Lett.* **25**, 1049 (2000).

47. W. Watanabe, Y. Masuda, H. Arimoto and K. Itoh, *Opt. Rev.* **6,** 167 (1999).

48. W. Watanabe and K. Itoh, *Jpn. J. Appl. Phys.* **40,** 592 (2001).

49. C. Corsi, A. Tortora and M. Bellini, *Appl. Phys. B* **77,** 285 (2003).

50. C. Corsi, A. Tortora and M. Bellini, *Appl. Phys. B* **78,** 299 (2004).

51. C. Corsi and M. Bellini, *Appl. Phys. B* **78**, 31 (2003).

52. J. K. Ranka, R. S. Windeler and A. J. Stentz, *Opt. Lett.* **25**, 25 (2000).

53. S. A. Diddams, D. J. Jones, J. Ye, S. T. Cundiff, J. L. Hall, J. K. Ranka, R. S. Windeler, R. Holzwarth, T. Udem and T. W. Hänsch, *Phys. Rev. Lett.* **84,** 5102 (2000).

54. J. Reichert, M. Niering, R. Holzwarth, M. Weitz, Th. Udem and T. W. Hänsch, *Phys. Rev. Lett.* **84**, 3232 (2000).

55. M. Niering, R. Holzwarth, J. Reichert, P. Pokasov, Th. Udem, M. Weitz, T. W. Hänsch, P. Lemonde, G. Santarelli, M. Abgrall, P. Laurent, C. Salomon and A. Clairon, *Phys. Rev. Lett.* **84**, 5496 (2000).

56. D. J. Jones, S. A. Diddams, J. K. Ranka, A. Stentz, R. S. Windeler, J. L. Hall and S. T. Cundiff, *Science* **288**, 635 (2000).

57. A. Baltuška, Th. Udem, M. Uiberacker, M. Hentschel, E. Goulielmakis, Ch. Gohle, R. Holzwarth, V. S. Yakovlev, A. Scrinzi, T. W. Hänsch and F. Krausz, *Nature* **421**, 611 (2003).

58. M. Hentschel, R. Kienberger, Ch. Spielmann, G. A. Reider, N. Milosevic, T. Brabec, P. Corkum, U. Heinzmann, M. Drescher and F. Krausz, *Nature* **414,** 509 (2001).

59. T. Brabec and F. Krausz, *Rev. Mod. Phys.* **72**, 545 (1999).

60. G. G. Paulus, F. Grasbon, H. Walther, P. Villoresi, M. Nisoli, S. Stragira, E. Priori and S. D. Silvestri, *Nature* **414,** 182 (2001).

61. D. B. Milosevic, G. G. Paulus and W. Becker, *Phys. Rev. Lett.* **89,** 153001 (2002).

Springer

http://www.springer.com/978-0-387-23294-2

Femtosecond Laser Spectroscopy
Hannaford, P. (Ed.)
2005, XX, 334 p.,
ISBN: 978-0-387-23294-2